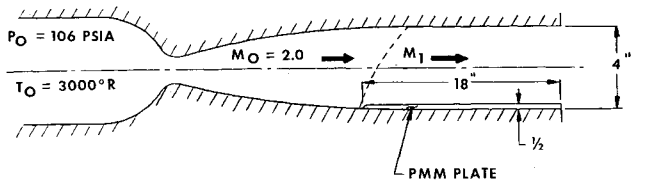

Fig. 2 Schematic of flat-plate test apparatus.

this mode of combustion and gain insight into the magnitude of the pressure increases obtainable.

Experimental Techniques

The experimental program was conducted in a Mach number 2.0, combustion heated, blowdown wind tunnel at nominal stagnation conditions of 106 psia and 1400° to 3300°R. Make-up oxygen was added to provide vitiated air with the correct proportion of atmospheric oxygen. A schematic of the experimental apparatus is shown in Fig. 2. The test section was a 4-in. square, and on one wall a $\frac{1}{2}$-in.-thick PMM plate was mounted. The plate was 18 in. long, 4 in. wide, and had a rounded leading edge. Since the tests were of short duration, and the amount of PMM ablated was small, the phenomenon was considered to be occurring in a constant-area duct. Pressure taps were located on the surface of the model and along the top wall of the test section. The leading edge of the plate produced a curved oblique shock which reflected from the tunnel wall and the plate.

Results

The pressures measured during the test are shown in Fig. 3 and are expressed as pressure coefficients referenced to test section conditions $C_p = (P - P_0)/q_0$ where the subscript 0 denotes freestream conditions. The test labeled "without burning" was run at a stagnation temperature that was high enough to permit ablation but low enough to preclude burning (T_T = 2100°R). An additional test made with cold dry air (T_T = 500°R), so that no ablation occurred, resulted in approximately the same pressures as the test with ablation but no burning. The test labeled "with burning" was run at a stagnation temperature of approximately 3000°R. The occurrence of burning was verified by photographs taken during the test. The difference in measured pressures shown in Fig. 3 (ΔC_p = 0.30 at the end of the plate) is due to combustion of the PPM albation products in the freestream air.

Theoretical calculations of the pressure rise due to combustion of the ablator were made, based on a one-dimensional constant-area heat addition process. The calculations depend on the Mach number M_1 in the constant-area duct at the start of burning. This Mach number is determined by the reduction in area from the test section to the duct and by the recovery η_R of the shocks and reflections produced by the curved leading edge of the plate, that is, the ratio of the total pressures across the shock system. A recovery of 0.80 to 0.85 approximates the pressure loss resulting in M_1 around 1.6. However, since the recovery is not known exactly, M_1

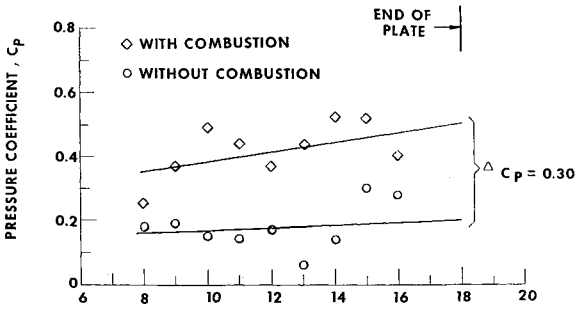

Fig. 3 Experimental values of pressure coefficient on a PMM flat plate.

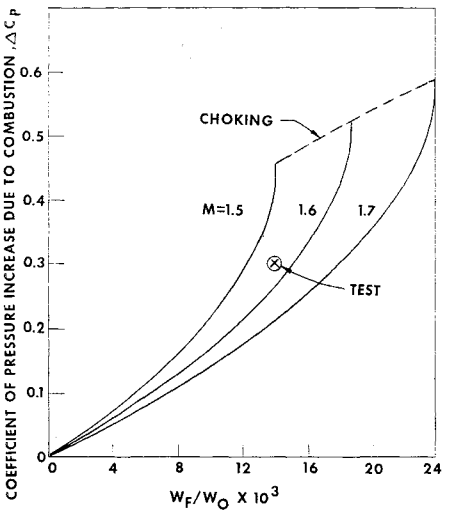

Fig. 4 Combustion ablator fuel/air ratio.

is retained as a parameter in presenting results. The results of the theoretical calculations of the constant-area burning process are shown in Fig. 4 as curves of the pressure rise coefficient ΔC_p vs the ratio of fuel flow to airflow W_f/W_0. The test point indicates the measured value of ΔC_p as deduced from Fig. 3. The test value of W_f/W_0 was determined from the ablation rate W_f and the measured tunnel flow W_0. The ablation rate was determined by weighing the plexiglas plate before and after the test and dividing the difference in weight by the time duration of the test. The results show that the test point is in close agreement with the theoretical results, thereby indicating a relatively efficient combustion process.

In summary, the tests and analysis described herein simulate a rudimentary combustor and provide limited confirmation of the feasibility of utilizing ablative materials as fuels for hypersonic airbreathing propulsion systems.

Reference

[1] Spadaccini, L. and Chinitz, W., "The Combustion of Solid Fuels in a High Temperature Supersonic Air Stream," *AIAA Journal*, Vol. 7, No. 9, Sept. 1969, pp. 1682–1687.

Effective Viscosity in a Turbulent Boundary Layer

S. W. CHI* AND C. C. CHANG†
The Catholic University of America, Washington, D.C.

Nomenclature

C = constant, Eq. (2)
C_f = frictional drag coefficient defined as $2\tau_s/\rho u_G^2$
K = constant, Eq. (1)
l = Prandtl's mixing length, Eq. (7)
P = constant, Eq. (1)
Re_2 = Reynolds number based upon momentum thickness, Eq. (3)
u = velocity in x direction, Eq. (4)
u_G = u in the mainstream
u^+ = nondimensional velocity defined as $u/(\tau_s/\rho)^{1/2}$, Eq. (1)

Received February 3, 1969; revision received June 23, 1969. This work is supported by a National Science Foundation Grant.

* Assistant Professor, Department of Space Science and Applied Physics.
† Professor and Head, Department of Space Science and Applied Physics.

u_G^+ = nondimensional velocity defined as $u_G/(\tau_s/\rho)^{1/2}$, Eq. (1)
v = velocity in y direction, Eq. (4)
x = distance measured along the plate, Eq. (4)
y = distance normal to the plate, Eq. (4)
y^+ = nondimensional distance defined as $y(\tau_s\rho)^{1/2}/\mu$, Eq. (1)
α = constant, Eq. (3)
β = constant, Eq. (3)
γ = constant, Eq. (10)
δ = boundary-layer thickness
η = nondimensional y defined as y/δ, Eq. (1)
ρ = density, Eq. (5)
μ = laminar dynamic viscosity, Eq. (10)
μ_{eff} = effective dynamic viscosity, Eq. (10)
τ = shear stress, Eq. (4)
τ_s = shear stress at the wall, Eq. (6)

A QUANTITATIVE degree of understanding of the behavior of turbulent boundary layers began with Prandtl[1] and von Kármán.[2] Confidence was established in the law of wall. Complementing the law of wall the work of Clauser[3] and Coles[4] established the outer defect profiles. Following these studies, the turbulent boundary-layer mean velocity data can be correlated by the similarity law to a high degree of accuracy. The present Note describes an examination of the existing mean velocity data for flat plate and presents an analysis that yields a continuous eddy viscosity described by a single equation.

Experimental data

Careful and extensive measurements of mean velocity profile on smooth flat plate with a turbulent boundary layer have been reported by several investigators, Schultz-Grunow,[5] Wieghardt and Tillmann,[6,4] Hama,[7] and Klebanoff and Diehl.[8] These data are correlated by the Coles' similarity formula,

$$u_G^+ - u^+ = -(1/K)\ln(\eta) + (P/K)[1 + \cos(\pi\eta)] \quad (1)$$

where the best values of K and P are found by the present authors to be 0.39 and 0.36, respectively.

In accordance with Coles,[4] the mean velocity profile may also be written

$$u^+ = (1/K)\ln(y^+) + C + (P/K)[1 - \cos(\pi\eta)] \quad (2)$$

in which K and P are the same constants as mentioned previously and C is a constant the magnitude of which can be determined from u^+ and y^+ data or alternatively from u_G^+

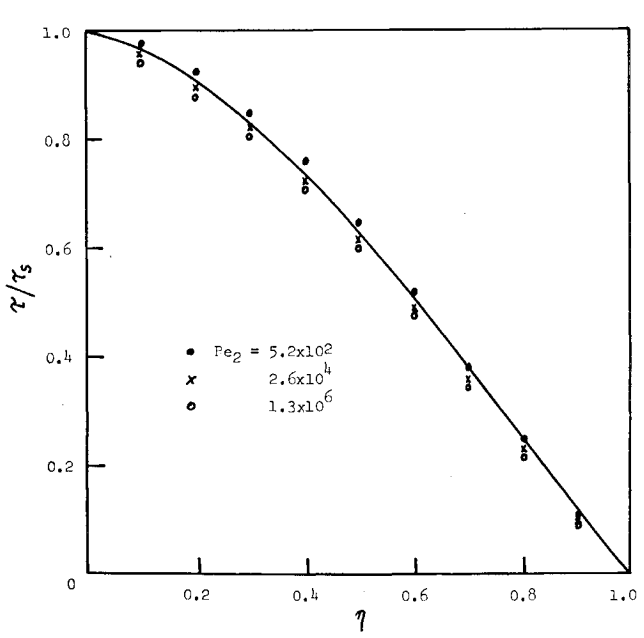

Fig. 1 Computed shear-stress distribution at various Reynolds numbers. ——, Eq. (8).

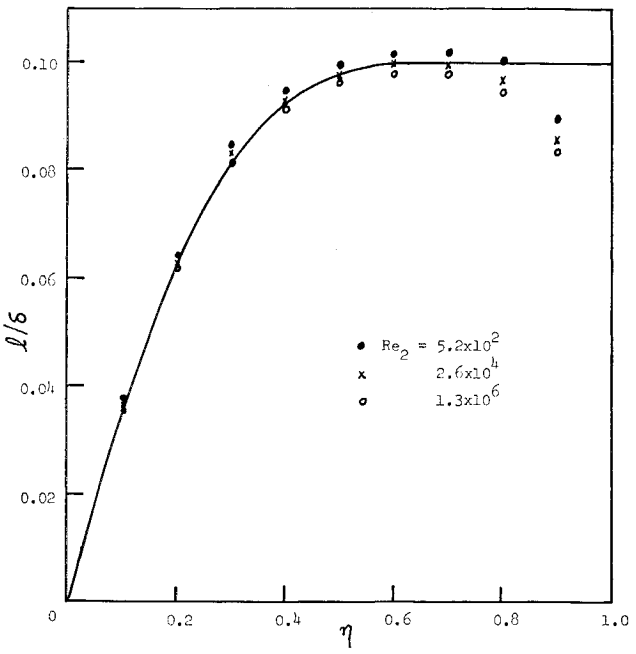

Fig. 2 Computed Prandtl's mixing length at various Reynolds numbers.—, Eq. (9).

[$\equiv(2/C_f)^{1/2}$] vs Re_2 data. We shall derive the best value of C from the latter data collected by Spalding and Chi.[9]

Using Eq. (1) and the definition for Re_2, one obtains

$$Re_2 = [(1 + P)/K - 2(1 + \alpha P + \beta P^2)/(K^2 u_G^+)]\exp[Ku_G^+ - (2P + KC)] \quad (3)$$

where the values of α and β are equal to 1.6 and 0.75, respectively. It has been found that a good correlation of u_G^+ vs Re_2 data by Eq. (3) is obtained at $C = 5.2$.

Evaluation of Shear Stress and Prandtl's Mixing Length

The equations of motion for the mean velocity on a flat plate may be written

$$(\partial u/\partial x) + (\partial v/\partial y) = 0 \quad (4)$$

and

$$u(\partial u/\partial x) + v(\partial u/\partial y) = \partial(\tau/\rho)/\partial y \quad (5)$$

Substituting Eq. (1) into Eqs. (4) and (5), after somewhat lengthy but straightforward manipulations, one obtains the following shear-stress formula:

$$\tau/\tau_s = 1 + \left\{Ku^+\eta + (Ku^+ - 2)\int_0^\eta Ku^+ d\eta - 2\int_0^\eta (Ku^+)^2 d\eta + \pi P(1 + Ku_G^+)Ku^+\int_0^\eta \eta\sin(\pi\eta)d\eta - 2\pi P(1 + Ku_G^+)\int_0^\eta Ku^+\eta\sin(\pi\eta)d\eta\right\} \Big\backslash \left\{(Ku_G^+)^2(1 + P) - 4Ku_G^+(1 + \alpha P + \beta P^2) + 2(1 + \alpha p + \beta P^2)\right\} \quad (6)$$

In Eq. (6), u^+ is a function of η, which is given by Eq. (1), and u_G^+ is a function of Re_2, which is given by Eq. (3). Hence, for a given value of Re_2 the shear-stress distribution τ/τ_s vs η can be calculated from Eq. (6), with the aid of Eqs. (1) and (3), in a straight forward manner. Figure 1 shows the calculated τ/τ_s vs η at several values of Re_2.

In the analysis of turbulent shear flow, it is common to postulate a relationship between the local shear stress and the velocity gradient. Taking into consideration the region outside the wall influence, the Prandtl's mixing-length hypothesis can be written

$$l/\delta = (\tau/\tau_s)^{1/2}/(du^+/d\eta) \quad (7)$$

Combination of Eqs. (1, 6, and 7) yields an expression for the

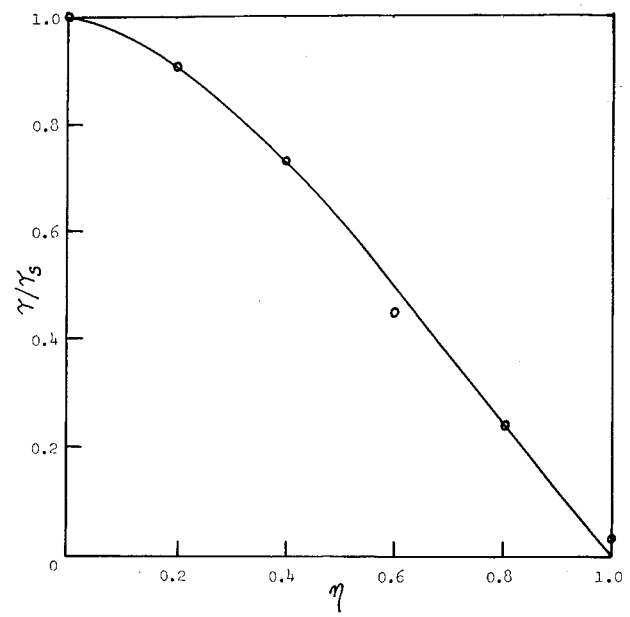

Fig. 3 Comparison of the computed and measured shear-stress distributions. O, experiments at $Re_2 = 1.24 \times 10^4$; ——, Eq. (8).

mixing length, which for brevity is not written out here in full. However, the calculated values of l/δ vs η at several values of Re_2 are shown in Fig. 2.

Turbulent Boundary-Layer Effective Viscosity

It can be seen in Figs. 1 and 2 that τ/τ_s and l/δ are, respectively, weak functions of Reynolds number. For practical purposes, it is convenient and sufficiently accurate to express τ/τ_s and l/δ as functions of η only. These functions can be represented by

$$\tau/\tau_s = 1 - 2\eta^2 + \eta^3 \tag{8}$$

and

$$l/\delta = 0.4\eta - 0.5\eta^2 + 0.2\eta^3 \tag{9}$$

within an accuracy of about $\pm 3\%$, as can be seen in Figs. 1 and 2.

In order to derive an analytical expression for the effective viscosity which is also valid for the region close to the wall, it is necessary to estimate the effect of viscous damping on the mixing length and the molecular viscosity. Accepting van Driest's[10] conclusion, our effective viscosity expression, following Eq. (9), can be written as

$$\mu_{\text{eff.}} = \mu + \rho\{\delta(0.4\eta - 0.5\eta^2 + 0.2\eta^3)[1 - \exp(-\gamma\delta^+\eta)]\}^2|\partial u/\partial y| \tag{10}$$

in which γ is a constant. Its appropriate value has been found to be 0.05.

Results and Conclusion

Existing mean velocity data for incompressible turbulent boundary layer on a flat plate were examined and correlated by the Coles' similarity formula. Based upon the correlated mean velocity data, the boundary-layer equations were solved for the shear-stress and the Prandtl's mixing-length distributions.

An analysis of the computed shear-stress and mixing-length profiles was made. It was found that 1) the shear-stress distribution can be represented by Eq. (8) and that 2) the turbulent boundary-layer effective viscosity can be represented by a single analytical expression of Eq. (10).

The comparison between Eq. (8) and the experimentally measured shear stresses, using hot wire technique, is shown in Fig. 3. The data, which were taken from Klebanoff,[11] are in good agreement with the present computation, as can be seen in Fig. 3.

Combining the definition for the effective viscosity $\tau = \mu_{\text{eff}}(\partial u/\partial y)$ with Eqs. (8) and (10), it can readily be shown that the mean velocity distribution based upon the present effective viscosity can be calculated by

$$u^+ = \int_0^\eta \frac{2\delta^+(1 - 2\eta + \eta^3)d\eta}{1 + (1 + 4(\delta^+)^2(1 - 2\eta + \eta^3)\{(0.4\eta - 0.5\eta^2 + 0.2\eta^3)[1 - \exp(-0.05\delta^+\eta)]\}^2)^{1/2}} \tag{11}$$

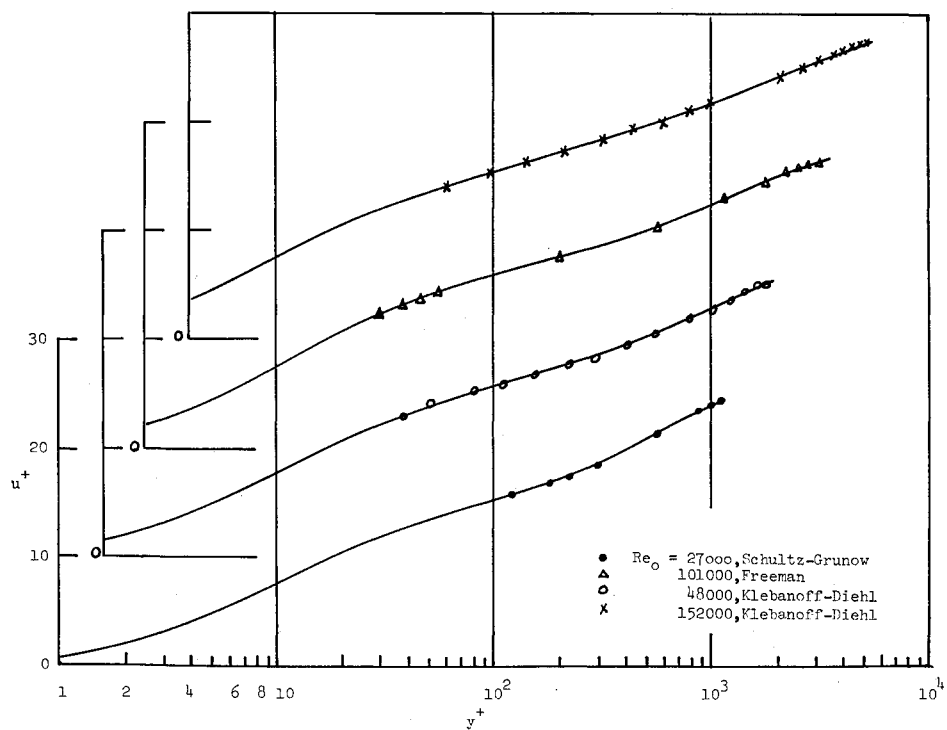

Fig. 4 Comparison between the predicted and the measured velocity profiles. ——, Eq. (11).

The agreement between the mean velocity profiles computed from Eq. (11) and the experiments of Schultz-Grunow,[5] Freeman, and Klebanoff and Diehl,[8] is remarkably good at all Reynolds number values as can be seen in Fig. 4.

References

[1] Prandtl, L., "Über die Ausgebildete Turbulenz," *Zeitschrift für Angewandte Mathematik und Physik*, Vol. 5, 1925, p. 136.

[2] von Kármán, T., "Mechanische Ahnlichkeit und Turbulenz," *Proceedings of the Third International Congress on Applied Mechanics*, Vol. 1, 1931, pp. 85–93.

[3] Clauser, F. H., "Turbulent Boundary Layers in Adverse Pressure Gradient," *Journal of the Aerospace Sciences*, Vol. 21, 1954, pp. 91–108.

[4] Coles, D., "The Young Person's Guide to the Data," Air Force Office of Scientific Research Internal Flow Program Stanford Conference, 1968.

[5] Schultz-Grunow, F., "New Frictional Resistance Law for Smooth Plates," TM 986, 1941, NACA.

[6] Wieghardt, K. and Tillman, W., "On the Turbulent Friction Layer for Rising Pressure," TM 1314, 1951, NACA.

[7] Hama, F. R., "The Turbulent Boundary Layer along a Flat Plate, I and II," *Reports of the Institute of Science and Technology, University of Tokyo*, Vol. 1, 1947, pp. 13–19.

[8] Klebanoff, P. S. and Diehl, Z. W., "Some Features of Artificially Thickened Fully Developed Turbulent Boundary Layers with Zero Pressure Gradient," TN 2475, 1951, NACA.

[9] Spalding, D. B. and Chi, S. W., "The Drag of a Compressible Turbulent Boundary Layer on a Smooth Flat Plate with and without Heat Transfer," *Journal of Fluid Mechanics*, Vol. 18, Pt. 1, 1964, pp. 117–143.

[10] van Driest, E. R., "On Turbulent Flow near a Wall," *Journal of the Aerospace Sciences*, Vol. 23, 1956, pp. 1007–1011, 1036.

[11] Klebanoff, P. S., "Characteristics of Turbulence in a Boundary Layer with Zero Pressure Gradient," TR 1247, 1955, NACA.

An Experimental Study of a Yawed Circular Cone in Hypersonic Flows

Y. Y. Chan*

National Aeronautical Establishment, Ottawa, Canada

In recent years, flowfields over conical bodies can be calculated to some extent because of the advance in computational techniques. These computational methods give information on a more general condition which is no longer a small perturbation from a known flowfield at zero incidence. For a cone at incidences in a supersonic stream one may calculate the inviscid flowfield up to the relative incidence $\alpha/\theta c$ where α is the angle of attack and θc is the semiapex angle of a cone, about unity until either the cross-flow velocity component (in a spherical polar coordinate system with the cone apex at the origin) reaches supersonic locally, at which imbedded shock waves may be formed, or the vortical singularity at the leeward generator leaves the surface.[1–3] The laminar compressible boundary-layer flow over the cone surface may also be computed from the most forward generator towards the lee side of the cone until the boundary layer separates from the surface.[4–8] These methods for boundary-layer computations can be applied up to a moderate angle of attack of the cone and require only the knowledge of pressure distributions on the cone surface, provided that the vorticity interaction close to the most windward generator is small and negligible.

The aim of the present work is to determine experimentally some flow quantities, such as static pressure distributions, heat-transfer distributions, and flow directions on the surface of a cone at moderate angle of attack. From these results the range of application of these advanced methods of computation for both inviscid and boundary-layer flows are assessed.

Received March 12, 1969; revision received June 30, 1969.

* Associate Research Officer, High Speed Aerodynamics Section. Member AIAA.

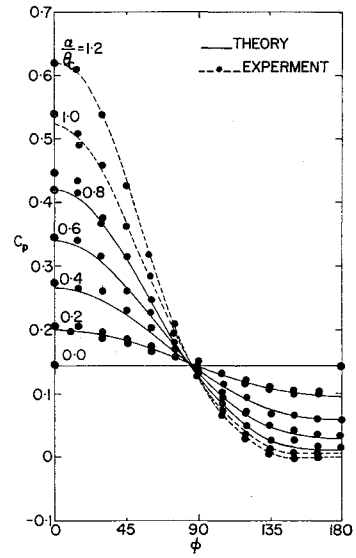

Fig. 1 Pressure distributions on a 15° circular cone at $M_\infty = 10.4$, $Re_{\infty x} = 10^6$.

Experimental Methods

Measurements were made on a right circular cone with a semiapex angle of 15°. The model is 4 in. long and the measuring station is located at $3\frac{1}{2}$ in. away from the apex so that the effect of self-induced pressure interaction at hypersonic speed is negligible at the present testing condition. The pressure measurements were made by small variable reluctance pressure transducers located inside the model as close as possible to the measuring holes. The heat-transfer measurements were made by heat-transfer gages of thin film thermometer type placed along the cone generator. The oil dots technique was used for surface flow visualization. The directions of the surface flow were then measured from the flow patterns.

The experiments were performed in the National Aeronautical Establishment hypersonic gun tunnel. The Mach number in the test section was 10.4 and the Reynolds number was 3.7×10^6/ft. The wall-to-stagnation temperature ratio was 0.23 and the boundary layers were laminar for these conditions. The model was pitched at relative incidences up to 1.2 with 0.2 steps. Surface pressure and heat-transfer distributions were measured at 15° circumferential angle steps around the cone.

Results and Discussion

With the assumption of high Reynolds number flow, the theoretical results for the inviscid and the viscous flows could be computed separately. The inviscid flowfields were calculated by the method of Ref. 3 for different relative incidences until local supersonic crossflow occurred (at $\alpha/\theta c$ about unity for the present conditions). The resulting pressure distributions from the inviscid flow model were then used to compute the boundary-layer flows by the method of Ref. 7.

The pressure distributions on the cone surface at different relative incidences are shown in Fig. 1. The over-all agreement between the computed pressure distributions and the experimental results is very good. At relative incidences of 0.6 and 0.8, the measured pressure is slightly higher than the theoretical curve at the circumferential angle ϕ near and at 180° (where ϕ is measured from the most windward generator of the cone). This is due to the piling up of vortical fluid in this region and to the displacement of the viscous flow effectively changing the local pressure distribution as observed in Refs. 9 and 10. At $\alpha/\theta c = 0.8$, the pressure minimum starts